



Dynamical Dark Energy in Light of Cosmic Distance Measurements. II. A Study Using Current Observations

Xiaoma Wang^{1,2}, Gan Gu^{1,2}, Xiaoyong Mu^{1,2}, Shuo Yuan¹, and Gong-Bo Zhao^{1,2,3}

¹ National Astronomical Observatories, Chinese Academy of Sciences, Beijing 100101, China; gbzhao@nao.cas.cn

² University of Chinese Academy of Sciences, Beijing 100049, China

³ Institute for Frontiers in Astronomy and Astrophysics, Beijing Normal University, Beijing 102206, China

Received 2024 April 9; accepted 2024 April 15; published 2024 May 20

Abstract

We extract key information on dark energy from current observations of BAO, OHD and H_0 , and find hints of dynamical behavior of dark energy. In particular, a dynamical dark energy model whose equation of state crosses -1 is favored by observations. We also find that the Universe has started accelerating at a lower redshift than expected.

Key words: Cosmology – (cosmology:) dark energy – cosmology: observations

1. Introduction

The physical origin of the cosmic acceleration remains veiled since its discovery in 1998 from observations of Type Ia supernovae (SNe Ia) (Riess et al. 1998; Perlmutter et al. 1999). Among all possible mechanisms, dark energy (DE) (Copeland et al. 2006) and modified gravity (MG) (Clifton et al. 2012) are two primary scenarios that have been extensively studied. Both DE and MG models can yield the same accelerating expansion of the Universe after the required tuning, and the expansion rate of the Universe is determined by the equation of state (EoS) w of an effective dark fluid.

The EoS is generally a function of time, expressed by the scale factor a or redshift z , and it is a ratio between the pressure P and ρ of the effective dark fluid. It is important to extract information of $w(z)$ from observations, because different DE or MG models can in principle be differentiated using the behavior of $w(z)$. The Λ CDM model, in which DE is the vacuum energy, predicts $w = -1$. Although still allowed by observations, this model suffers from serious theory problems (Weinberg 1989), and has been challenged by the “Hubble tension” (Di Valentino et al. 2021). In alternative models, w generally evolves with time. For example, the single-scalar-field models of quintessence (Ratra & Peebles 1988) and phantom (Caldwell 2002) predict $w > -1$ and $w < -1$ during the evolution, respectively, and in models with intrinsic degrees of freedom such as quintom (Feng et al. 2005), w can cross the -1 boundary.

Observations of the cosmic distances, such as the baryonic acoustic oscillations (BAO) (Eisenstein & Hu 1998; Cole et al. 2005; Eisenstein et al. 2005), are less subject to systematics compared to probes of the cosmic structure formation, and the behavior of $w(z)$ directly affects the cosmic distances, therefore

the distance measurements are ideal observables for DE studies.

In this work, we learn the behavior of $w(z)$ from current measurements of the cosmic distances based on the method developed in a companion paper (Gu et al. 2024), and find hints of interesting features of $w(z)$. We present the method and data used in this analysis in Section 2, show the results in Section 3 and conclude in Section 4.

2. Method and Data

In this section, we briefly describe the method used for this work, as developed in a companion paper (Gu et al. 2024), and the data sets used for the analysis.

We start from parameterizing the angular diameter distances⁴ following Zhu et al. (2015),

$$\frac{D_A(z)}{D_{A,\text{fid}}(z)} = \alpha_0 \left(1 + \alpha_1 x + \frac{1}{2} \alpha_2 x^2 + \frac{1}{6} \alpha_3 x^3 + \frac{1}{24} \alpha_4 x^4 \right), \quad (1)$$

where $1 + x \equiv D_{A,\text{fid}}(z)/D_{A,\text{fid}}(z_*)$, and subscript “fid” denotes the fiducial model, which is chosen to be a flat Λ CDM model with $\Omega_M = 0.3153$ as favored by the Planck observations (Aghanim et al. 2020). The quantity z_* is the pivot redshift set to 0.5 in this work.⁵ The Hubble expansion rate H can be

⁴ For current data, we find that keeping the expansion up to the x^4 term is a reasonable choice to balance between the bias and uncertainty of the reconstruction.

⁵ The choice of z_* can be arbitrary in principle, and it has almost no impact on the final reconstruction result, as demonstrated in Gu et al. (2024).

Table 1
A List of BAO Datasets Used in This Work

Survey	z_{eff}	D_V/r_d	D_A/r_d	D_H/r_d	Reference
SDSS MGS	0.15	4.47 ± 0.17	Ross et al. (2015)
BOSS	0.38	...	10.23 ± 0.17	25.00 ± 0.76	Alam et al. (2017)
BOSS	0.51	...	13.36 ± 0.21	22.33 ± 0.58	Alam et al. (2017)
eBOSS LRG	0.70	...	17.86 ± 0.33	19.33 ± 0.53	Bautista et al. (2020)
eBOSS ELG	0.85	$18.33^{+0.57}_{-0.62}$	de Mattia et al. (2021)
eBOSS Quasar	1.48	...	30.69 ± 0.80	13.26 ± 0.55	Neveux et al. (2020)
eBOSS Ly α	2.33	...	37.6 ± 1.9	8.93 ± 0.28	du Mas des Bourboux et al. (2020)
6dFGS	0.106	2.976 ± 0.133	Beutler et al. (2011)
WiggleZ	0.44	11.495 ± 0.556	Kazin et al. (2014)
WiggleZ	0.60	14.878 ± 0.677	Kazin et al. (2014)
WiggleZ	0.73	16.854 ± 0.576	Kazin et al. (2014)
DES Y3	0.835	...	18.92 ± 0.51	...	Abbott et al. (2022)

obtained using the relation between H and D_A , namely,

$$\frac{H_{\text{fid}}(z)}{H(z)} = \alpha_0 [1 + \alpha_1 + (2\alpha_1 + \alpha_2)x + \left(\frac{3}{2}\alpha_2 + \frac{1}{2}\alpha_3\right)x^2 + \left(\frac{2}{3}\alpha_3 + \frac{1}{6}\alpha_4\right)x^3 + \frac{5}{24}\alpha_4x^4]. \quad (2)$$

The free parameters α_i can be determined by fitting Equations (1) and (2) to distance measurements, generally including BAO and supernovae distances, the observational Hubble data (OHD) (Stern et al. 2010) and so forth. Ultimately we can obtain a DE shape function defined as,

$$S[f(a)] \equiv \frac{f(a) - f(a_*)}{f'(a_*)}, \quad f(a) \equiv AH^2a^3 = B[Xa^3] + C. \quad (3)$$

Throughout the paper, the prime denotes a derivative with respect to the scale factor a , and X is the DE density normalized to unity today.⁶ By design, $S[f(a)]$ extracts the shape of Xa^3 from data, thus constants A , B , C are irrelevant.⁷ A few important functions that are directly related to DE can be derived from f , including the normalized DE pressure function,

$$\frac{P}{P(a_*)} \equiv \frac{a_*^2}{a^2} \cdot \frac{f'(a)}{f'(a_*)} = \frac{w(a)X(a)}{w(a_*)X(a_*)}, \quad (4)$$

and the DE characterization function,

$$g(a) \equiv -\frac{1}{3} \left(1 + a \frac{f''(a)}{f'(a)} \right) = w - \frac{a}{3} \frac{w'}{w}. \quad (5)$$

⁶ Note that when fitting the α 's in Equations (1) and (2) to distance measurements, the derived X may not be positive-definite. Therefore when deriving quantities related to f' including the pressure function and the g function, we apply a prior of $X > 0$. We check the posteriors and find that this has a marginal effect on the final result.

⁷ For BAO measurements, $A = r_d^2$, $B = AH_0^2(1 - \Omega_M)$, $C = AH_0^2\Omega_M$ where r_d is the sound horizon at decoupling, but these constants have no impact on S , $P/P(a_*)$, $g(a)$ and $q(a)$ by design.

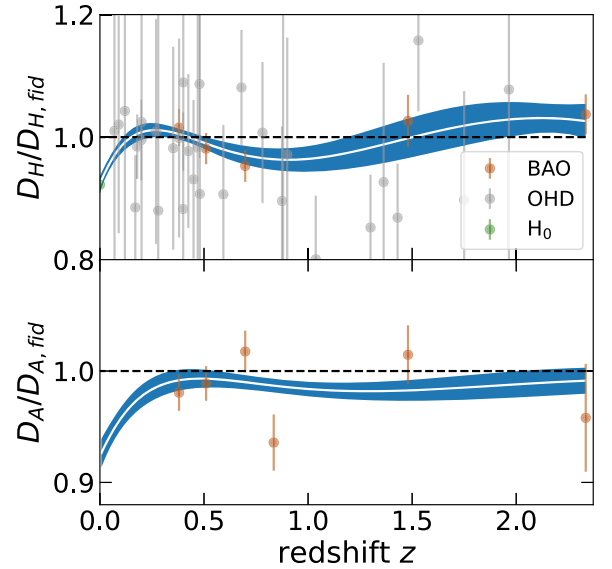


Figure 1. The mean (white curves) and 68% CL uncertainties of the reconstructed $D_H/D_{H,\text{fid}}$ and $D_A/D_{A,\text{fid}}$ using the combined data set of BAO, OHD and H_0 measurements shown as data points. The horizontal dashed lines signify $D_H/D_{H,\text{fid}} = D_A/D_{A,\text{fid}} = 1$ for a reference.

Given $g(a)$, a general solution to the differential Equation (5) is,

$$w(a) = \frac{w(a_B)f_1(a_B, a)}{1 - w(a_B)f_2(a_B, a)}, \quad (6)$$

with

$$f_1(a_1, a_2) \equiv \exp \left[-3 \int_{a_1}^{a_2} \frac{g(x)}{x} dx \right],$$

$$f_2(a_1, a_2) \equiv 3 \int_{a_1}^{a_2} \frac{f_1(a_1, x)}{x} dx, \quad (7)$$

and $w(a_B)$ is the boundary condition at $a = a_B$.

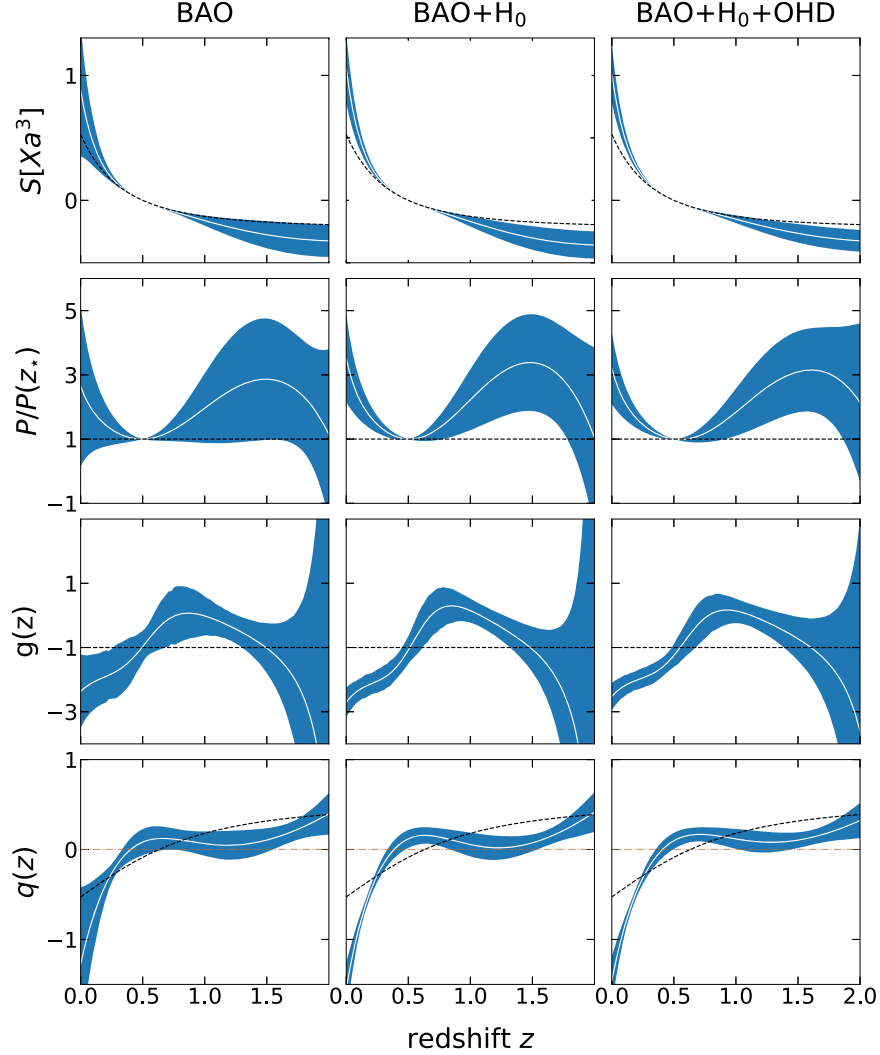


Figure 2. The mean (white curves) and 68% CL uncertainties (blue shaded regions) of the reconstructed DE shape function $S[Xa^3]$ (top panels); the normalized DE pressure function $P/P(z_*)$ (panels in the second row); the characterization DE function $g(z)$ (third row), and the deceleration function $q(z)$ of the Universe (bottom panels), derived from three different combinations of data sets illustrated in the legend. In all panels, the black dashed lines show the Λ CDM prediction, and the red dashed lines in the bottom panels signify $q = 0$ for a reference. The value of Ω_M is set to be 0.3153 when producing the Λ CDM prediction for $q(z)$.

In addition, the deceleration function of the Universe can also be derived from f , namely,

$$q(a) \equiv -\frac{a f'(a)}{2 f(a)} + \frac{1}{2}. \quad (8)$$

The data sets used in this work include the isotropic and anisotropic BAO measurements listed in Table 1⁸, the observational $H(z)$ data (OHD) measured using the ages of galaxies (Stern et al. 2010), compiled in Yu et al. (2018), and a

⁸ Note that the BOSS and WiggleZ surveys have a small overlapping region in footprint thus the BAO measurements from these two surveys are not strictly independent. But given the small overlapping area compared to the full footprint of BOSS, we assume that the cross-covariance in the measurements is negligible.

local measurement of $H_0 = 73.04 \pm 1.04 \text{ km s}^{-1} \text{ Mpc}^{-1}$ (Riess et al. 2022).

We use the `Cobaya` (Torrado & Lewis 2021) code to sample the parameter space of the α 's with the Markov Chain Monte Carlo (MCMC) algorithm, and perform the post-processing using the `Getdist` (Lewis 2019) software.

3. Results

Our main results are summarized in Figures 1–4.

Figure 1 shows the mean and 68% confidence level (CL) reconstructed $D_H \equiv c/H(z)$ (c is the speed of light) and D_A from the combined data set of BAO, OHD and H_0 measurements, rescaled by the prediction of the fiducial model. As

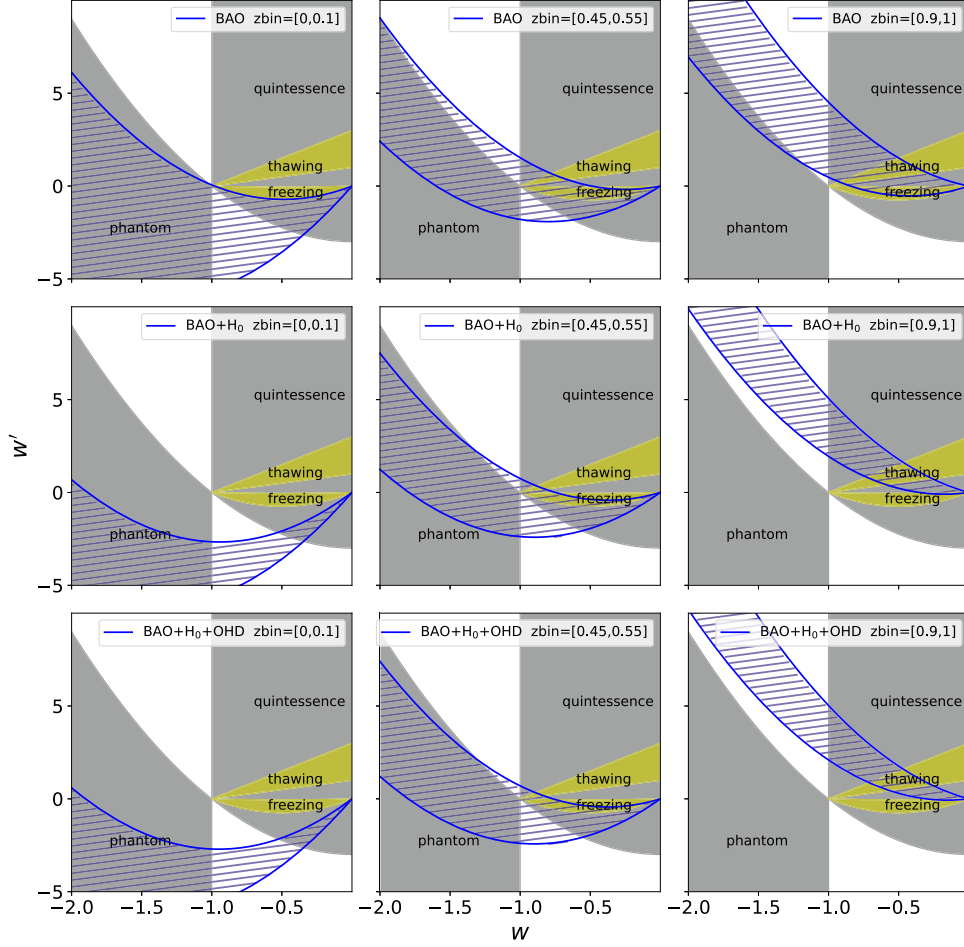


Figure 3. The $w - w'$ phase space diagram predicted by theory models (filled regions) and from observational constraints (hatched regions) through the reconstructed $g(z)$ function derived from three data combinations in three redshift intervals, as shown in the legend.

shown, the reconstructed functions significantly deviate from the fiducial Λ CDM model, and appear wiggly, which is primarily driven by both the H_0 and BAO measurements at low and intermediate redshifts, respectively.

Figure 2 turns the distance measurements into important functions that are directly related to physical features of DE. Panels in the top row show the reconstructed DE shape function, visualizing the time evolution of Xa^3 . Comparing to the Λ CDM prediction shown in the black dashed lines, we see that the BAO data tilt S around the pivot point of $z_p = 0.5$, namely, the BAO data tend to lift S up at $z < z_p$ and push S downwards at $z > z_p$. Interestingly, this feature is supported by both the H_0 and OHD measurements, namely, when H_0 and OHD are added to the analysis, the feature becomes more pronounced with much smaller uncertainties, which disfavors the Λ CDM model.

The $P/P(z_*)$ panels provide more information on DE. Specifically, we see that P has an apparent local minimum at around $z = 0.5$ when the H_0 and OHD measurements are

combined with the BAO data. This actually disfavors the w CDM model, in which P is a power-law function of a .

Further information on $w(z)$ can be learned from the reconstructed $g(z)$ function displayed in panels in the third row of Figure 2. This function shows a strong dynamical behavior in all cases, indicating an evolving $w(z)$. It is true that solving for $w(z)$ from $g(z)$ requires a boundary condition which is unknown, but we can still use the reconstructed $g(z)$ to identify the allowed region in the $w - w'$ phase space, which can in principle be used to differentiate DE models. The shaded area in Figure 3 illustrates the allowed parameter space by single scalar field models. Specifically, the quintessence (Ratra & Peebles 1988) and phantom (Caldwell 2002) models sit in regions of $w > -1 \cap w' > -3(1-w)(1+w)$ and $w < -1 \cap w' < -3(1-w)(1+w)$, respectively (Chiba 2006). The behavior of the quintessence model may be classified into two scenarios, namely, the thawing ($w \approx -1$ at high redshifts and grows later on) and freezing ($w > -1$ at high redshifts and decreases with time) cases, occupying the regions of

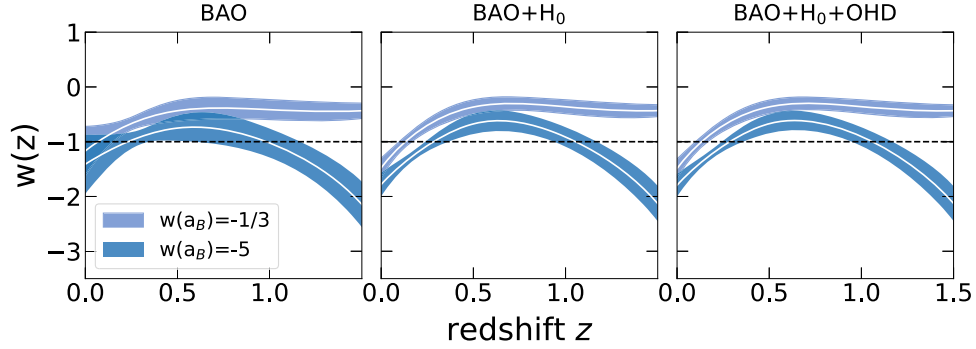


Figure 4. The mean and 68% CL reconstructed $w(z)$ by solving the differential equation using boundary conditions of $w(a_B) = -1/3$ and $w(a_B) = -5$, respectively, where $a_B = 0.35$. Results shown are derived from different data combinations illustrated in the legend.

$(1 + w) < w' < 3(1 + w)$ and $3w(1 + w) < w' < 0.2w(1 + w)$, respectively (Caldwell & Linder 2005). On the other hand, the reconstructed $g(z)$ function constrains the relation between w and w' in a given redshift range, thus we can use $g(z)$ to target the region in the phase space favored by observations. In Figure 2, the hatched regions are favored by observations (at 68% CL) derived from different data combinations in three redshift intervals, namely, $z \in [0, 0.1]$, $[0.45, 0.55]$ and $[0.9, 1.0]$. For all data combinations, we see a similar trend, namely, data favor the phantom model at $z < 0.1$, while at $0.9 < z < 1.0$, most of the data-favored region overlaps with the quintessence regime. This indicates an evolving $w(z)$ that crosses the -1 boundary during evolution, which is consistent with the prediction of the quintom model (Feng et al. 2005). We check this conclusion by directly solving the differential equation with two choices of boundary conditions, namely, $w(a_B) = -1/3$ and $w(a_B) = -5$ with $a_B = 0.35$, which are sufficiently extreme. The two solutions are depicted in Figure 4. In all cases, $w(z)$ tends to cross -1 during evolution, and the trend becomes significant when H_0 and OHD data sets are combined with the BAO data in the analysis.

Panels in the bottom row of Figure 2 show the reconstructed deceleration function $q(z)$. Comparing to the Λ CDM prediction with $\Omega_M = 0.3153$, we see that data favor a smaller z_{tr} , which is the redshift for the acceleration-deceleration transition, namely, $z_{tr} \approx 0.4$ while $z_{tr}(\Lambda\text{CDM}) \approx 0.6$. This means that the Universe starts accelerating much later than expected in the Λ CDM model.

4. Conclusion

Revealing the nature of DE is one of the most challenging tasks in modern physics. Equipped with high-quality observational data in this era of precision cosmology, we can use proper theoretical and numerical tools to extract crucial information on DE from observations, which can in principle offer important guidance for probing the new physics of DE.

In this work, we extract the DE shape function, pressure function, the characterization function and the cosmic

deceleration function from measurements of cosmic distances in recent years. Combining the observations of BAO, OHD and H_0 , we find that Λ CDM and w CDM models are disfavored, and a dynamical DE model with w crossing -1 is better supported by data. Interestingly, we find that the cosmic acceleration may have started much later than expected in the Λ CDM model.

Our method and pipeline are directly applicable to forthcoming distance measurements including BAO measurements from galaxy surveys such as DESI (Aghamousa et al. 2016; Adame et al. 2024), PFS (Ellis et al. 2014) and Euclid (Laureijs et al. 2011), supernovae surveys of LSST (LSST Science Collaboration et al. 2009) and Roman (Spergel et al. 2015) and so forth. These planned studies will further investigate the dynamical nature of w , which can deepen our understanding of DE.

Acknowledgments

We thank Ruiyang Zhao for helpful discussions. All authors are supported by the National Key R & D Program of China (2023YFA1607800 and 2023YFA1607803), National Natural Science Foundation of China (NSFC, Grant Nos. 11925303 and 11890691), and by a CAS Project for Young Scientists in Basic Research (No. YSBR-092). S.Y. is also supported by the National Natural Science Foundation of China (NSFC, Grant No. 12203062). S.Y. and G.B.Z. are also supported by science research grants from the China Manned Space Project with No. CMS-CSST-2021-B01. G.B.Z. is also supported by the New Cornerstone Science Foundation through the XPLORER prize.

References

- Abbott, T. M. C., Aguena, M., Allam, S., et al. 2022, *PhRvD*, **105**, 043512, *PhRvD*
- Adame, A. G., Aguilar, J., Ahlen, S., et al. 2024, arXiv:2404.03002
- Aghamousa, A., Aguilar, J., Ahlen, S., et al. 2016, arXiv:1611.00036
- Aghanim, N., Akrami, Y., Ashdown, M, et al. 2020, *A&A*, **652**, A6, [Erratum: *Astron.Astrophys.* 652, C4 (2021)]
- Alam, S., Ata, M., Bailey, S., et al. 2017, *MNRAS*, **470**, 2617
- Bautista, J. E., Paviot, R, Magaña, M.V, et al. 2020, *MNRAS*, **500**, 736
- Beutler, F., Blake, C., Colless, M., et al. 2011, *MNRAS*, **416**, 3017
- Caldwell, R. R. 2002, *PhLB*, **545**, 23

- Caldwell, R. R., & Linder, E. V. 2005, [PhRvL](#), **95**, 141301
- Chiba, T. 2006, [PhRvD](#), **80**, 063501, [Erratum: Phys.Rev.D 80, 129 901 (2009)]
- Clifton, T., Ferreira, P. G., Padilla, A., & Skordis, C. 2012, [PhR](#), **513**, 1
- Cole, S., Percival, W. J., Peacock, J. A., et al. 2005, [MNRAS](#), **362**, 505
- Copeland, E. J., Sami, M., & Tsujikawa, S. 2006, [IJMPD](#), **15**, 1753
- de Mattia, A., Ruhlmann-Kleider, V., Raichoor, A., et al. 2021, [MNRAS](#), **501**, 5616
- Di Valentino, E., Mena, O., Pan, S., et al. 2021, [CQGra](#), **38**, 153001
- du Mas des Bourboux, H., Rich, J., Font-Ribera, A., et al. 2020, [ApJ](#), **901**, 153
- Eisenstein, D. J., & Hu, W. 1998, [ApJ](#), **496**, 605
- Eisenstein, D. J., Zehavi, I., Hogg, D. W., et al. 2005, [ApJ](#), **633**, 560
- Feng, B., Wang, X.-L., & Zhang, X.-M. 2005, [PhLB](#), **607**, 35
- Gu, G., Wang, X., Mu, X., Yuan, S., & Zhao, G.-B. 2024, arXiv:2404.06303
- Kazin, E. A., Koda, J., Blake, C., et al. 2014, [MNRAS](#), **441**, 3524
- Laureijs, R., Amiaux, J., Arduini, S., et al. 2011, arXiv:1110.3193
- Lewis, A. 2019, arXiv:1910.13970
- LSST Science Collaboration, Abell, P. A., Allison, J., et al. 2009, arXiv:0912.0201
- Neveux, R., Burtin, E., de Mattia, A., et al. 2020, [MNRAS](#), **499**, 210
- Perlmutter, S., Aldering, G., Goldhaber, G., et al. 1999, [ApJ](#), **517**, 565
- Ratra, B., & Peebles, P. J. E. 1988, [PhRvD](#), **37**, 3406
- Riess, A. G., Filippenko, A. V., Challis, P., et al. 1998, [AJ](#), **116**, 1009
- Riess, A. G., Yuan, W., Macri, L.M., et al. 2022, [ApJL](#), **934**, L7
- Ross, A. J., Samushia, L., Howlett, C., et al. 2015, [MNRAS](#), **449**, 835
- Spergel, D., Gehrels, N., Baltay, C., et al. 2015, arXiv:1503.03757
- Stern, D., Jimenez, R., Verde, L., Kamionkowski, M., & Stanford, S. A. 2010, [JCAP](#), **02**, 008
- Takada, M., Ellis, R., Chiba, M., et al. 2014, [PASJ](#), **66**, R1
- Torrado, J., & Lewis, A. 2021, [JCAP](#), **2021**, 057
- Weinberg, S. 1989, [RvMP](#), **61**, 1
- Yu, H., Ratra, B., & Wang, F.-Y. 2018, [ApJ](#), **856**, 3
- Zhu, F., Padmanabhan, N., & White, M. 2015, [MNRAS](#), **451**, 236